Stellarator and tokamak plasmas: a comparison

2012 Plasma Phys. Control. Fusion 54 124009

(http://iopscience.iop.org/0741-3335/54/12/124009)

Plasma Phys. Control. Fusion **54** (2012) 124009 (12pp) doi:10.1088/0741-3335/54/12/124009

Stellarator and tokamak plasmas: a comparison

P Helander, C D Beidler, T M Bird, M Drevlak, Y Feng, R Hatzky, F Jenko, R Kleiber, J H E Proll, Yu Turkin and P Xanthopoulos

Max-Planck-Institut für Plasmaphysik, Greifswald and Garching, Germany

Received 22 June 2012, in final form 30 August 2012
Published 21 November 2012
Online at stacks.iop.org/PPCF/54/124009

Abstract
An overview is given of physics differences between stellarators and tokamaks, including magnetohydrodynamic equilibrium, stability, fast-ion physics, plasma rotation, neoclassical and turbulent transport and edge physics. Regarding microinstabilities, it is shown that the ordinary, collisionless trapped-electron mode is stable in large parts of parameter space in stellarators that have been designed so that the parallel adiabatic invariant decreases with radius. Also, the first global, electromagnetic, gyrokinetic stability calculations performed for Wendelstein 7-X suggest that kinetic ballooning modes are more stable than in a typical tokamak.

(Some figures may appear in colour only in the online journal)

1. Introduction

It has been said that, in the early days when fusion research was classified, much of the work was duplicated in various laboratories across the world, so that, for instance, the tokamak, the mirror machine and the Grad–Shafranov equation were invented or discovered independently in several places. But there was one exception: only Lyman Spitzer in Princeton was ingenious enough to think of the stellarator [1]. It has occupied an important position in the fusion programme for six decades now, but has spent much of that time in the shadow of its toroidal cousin, the tokamak. Perhaps for this reason, the physical properties of stellarators are less well known than they deserve to be. Historically, many key concepts in magnetic confinement physics originated from stellarators [2], and great strides have been taken in their development in recent years, making the stellarator a very serious candidate for a fusion reactor. In this paper we present an overview of similarities and differences between stellarator and tokamak plasmas, emphasizing conceptual and recent theoretical developments. No attempt is made to review the considerable body of experimental results that can be found in the literature. Most of the material can be found in other publications, but some of it is new, in particular in the section on microinstabilities.

2. Magnetic field

As Spitzer realized [3] and Mercier proved mathematically [4], there are three ways of producing a rotational transform of a toroidal magnetic field. From an expansion of Maxwell's equations in the vicinity of the magnetic axis, the average number of poloidal turns of a field line in one toroidal revolution can be expressed as an integral along the length l once around the magnetic axis [4, 5],

$$\iota = \frac{1}{q} = \frac{1}{2\pi}\int_0^L \left[\frac{\mu_0 J}{2B_0} - (\cosh\eta - 1)d' - \tau\right]\frac{\mathrm{d}l}{\cosh\eta} - N. \tag{1}$$

Here J is the current density on the magnetic axis, N is an integer of topological origin, $e^{\eta} = r_2/r_1$ the elongation of the flux surfaces, $\mathrm{d}(l)$ their tilting angle with respect to the curvature vector $\boldsymbol{\kappa} = \mathrm{d}\boldsymbol{b}/\mathrm{d}l$, where $\boldsymbol{b} = \boldsymbol{B}/B$ is the unit vector along the magnetic field $\boldsymbol{B}$, and $\tau(l) = (\mathrm{d}\boldsymbol{\kappa}/\mathrm{d}l)\cdot(\boldsymbol{b}\times\boldsymbol{\kappa})/\kappa^2$ denotes its torsion, see figure 1. The three ways of twisting the magnetic field are thus

- driving a toroidal current;
- elongating the flux surfaces and making them rotate poloidally as one moves around the torus;
- making the magnetic axis non-planar, so that $\tau \neq 0$.

Tokamaks and reversed field pinches use the first method, LHD uses the second one, TJ-II and Wendelstein 7-X the last two,

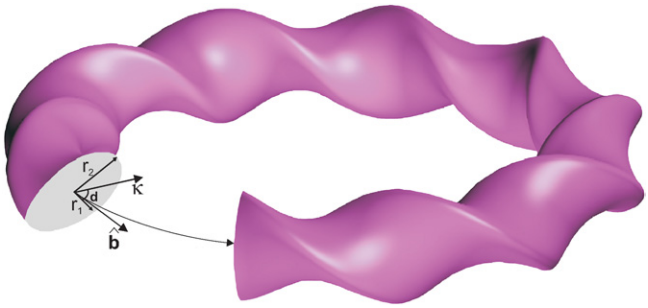

Figure 1. Flux-surface geometry in the vicinity of the magnetic axis of LHD. The rotational transform is generated by the poloidal rotation of the flux-surface cross section as one moves around the torus.

and NCSX all three. The last method alone was used by the first stellarators built in Princeton, which had circular cross section and the magnetic axis bent into the form of a figure eight.

The first method is simplest in the sense that it allows the device to be axisymmetric, making it easier to build, but suffers from the disadvantage of being non-steady-state or requiring non-inductive current drive. A further advantage of axisymmetry is that the existence of flux surfaces is guaranteed, whereas care is needed to avoid large magnetic islands and stochastic regions in non-axisymmetric magnetic fields.

3. Macroscopic equilibrium and stability

Avoiding a toroidal plasma current brings great advantages for plasma stability. Indeed, magnetohydrodynamic (MHD) stability plays a far less prominent role in stellarators than in tokamaks, where the toroidal current causes kink modes, sawteeth and resistive and neoclassical tearing modes that all limit the plasma performance. These instabilities are usually absent in stellarators for the simple reason that there is no, or very little, net toroidal plasma current.

There is, of course, a non-zero poloidal plasma current present to satisfy force balance, $\boldsymbol{J}\times\boldsymbol{B}=\nabla p$, and just like in a tokamak, the requirement $\nabla\cdot\boldsymbol{J}=0$ implies the existence of a Pfirsch–Schlüter current parallel to the magnetic field, since the perpendicular current $\boldsymbol{J}_\perp=(\boldsymbol{B}\times\nabla p)/B^2$ is generally not divergence-free. In addition, at low collisionality a bootstrap current arises for reasons similar to those in a tokamak, although the details are different because the particle orbits are not the same. The total toroidal current arising in this way is, however, usually substantially smaller than the typical (Ohmic) current in a tokamak. Of course, it is quite possible to drive a more substantial current using a transformer, and then tearing modes can be destabilized [6].

In principle neoclassical tearing modes can also exist in a stellarator, since these do not depend on a destabilizing Ohmic current profile for their existence but rather on a non-zero bootstrap current. The latter is reduced when a magnetic island forms and the pressure profile is flattened within it, and in tokamaks this negative current perturbation causes the island to grow further. In stellarators, however, the (global) magnetic shear usually has the opposite sign from that in tokamaks, so that, if an island should form and flatten the pressure profile, the resulting reduction in the bootstrap current makes the island shrink rather than grow. Neoclassical tearing modes are thus nonlinearly stable unless the bootstrap current is negative [7]. (The bootstrap current is taken to be positive if it increases the rotational transform.) In fact, finite plasma pressure often has the tendency to 'heal' magnetic islands in stellarators [8–10].

Stellarators do not experience plasma-terminating disruptions when, for instance, a stability limit is approached. The only exception seems to be situations where a transformer is used to induce so much toroidal current that tearing modes are destabilized [11]. After 120 000 plasma discharges, LHD has still not experienced a single current disruption [12].

In stellarators, the plasma density is not limited by the 'Greenwald' limit [13] but is instead determined by radiation losses from the plasma core. It is therefore a 'soft' limit and depends on the concentration and transport of impurities. Because the Greenwald limit is absent, stellarators often operate at a higher density than do tokamaks. The record is held by LHD, where densities $n_e=10^{21}\,\mathrm{m}^{-3}$ are reached in so-called super-dense core plasmas. The question why stellarators do not have a Greenwald limit cannot be answered without understanding its origin in tokamaks. A recent explanation by Gates and Delgado-Aparicio [14] suggests that the limit is due to the destabilization of magnetic islands (in the outer regions rather than the core) by radiation losses: at high enough density these cannot be overcome by local Ohmic heating, and this leads to further island growth. As the authors themselves note, this mechanism would not operate in stellarators.

The pressure limit is also approached in a different way from that in tokamaks. The limit set by pressure-driven MHD modes is surprisingly 'soft'; for instance, LHD routinely operates far above the ideal-MHD ballooning limit. It is not entirely clear why this is possible, but it appears that finite-Larmor-radius effects are playing a stabilizing role. Moreover, a significant fraction of the plasma pressure can be produced by suprathermal ions from neutral-beam injection, which has a stabilizing effect on ballooning modes [15]. By shaping the plasma appropriately, it is possible to raise the ideal ballooning limit significantly. In W7-X the volume-averaged normalized pressure limit is about $\langle\beta\rangle=5\%$. Because the stability limit is so high and soft, the *equilibrium* pressure limit is more important than in the tokamak. The Shafranov shift limits the pressure in a classical stellarator to about

$$\beta_{\max}\sim\frac{\iota^2}{2A},$$

where A denotes the aspect ratio. By optimizing the magnetic-field geometry so as to reduce the Pfirsch–Schlüter current, it is possible to reduce the Shafranov shift significantly, and this has been carried out successfully in the designs of W7-AS [11] and W7-X. Another equilibrium effect limiting the achievable pressure is the tendency of the magnetic field to become stochastic in the edge region at high beta. Figure 2 shows calculations of this effect in W7-X using the PIES code, which solves the force balance equation $\boldsymbol{J}\times\boldsymbol{B}=\nabla p$

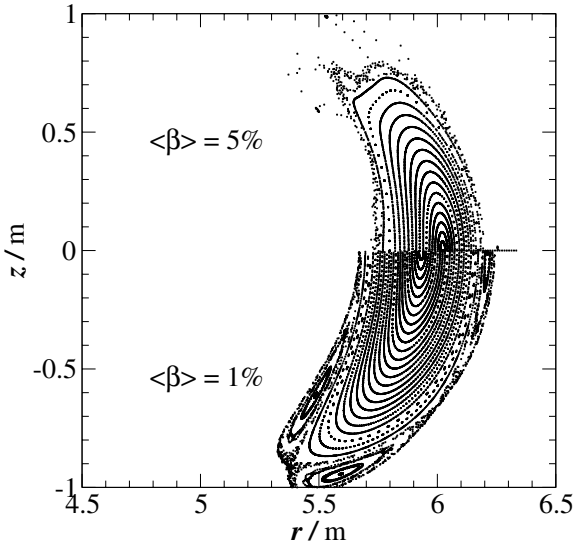

Figure 2. Poincaré sections of two equilibria in W7-X with different normalized pressures. The pressure profiles are in both cases of the form $p = p_0(1-s)(1-s^4)$, with s the normalized toroidal flux coordinate. The Shafranov shift and a stochastization of the edge region are clearly seen in the $\langle\beta\rangle = 5\%$ equilibrium.

without assuming nested flux surfaces [16]. As the volume-averaged normalized pressure $\langle\beta\rangle$ increases from 1% to 5%, the confinement region, i.e. the volume inside the largest closed flux surface, shrinks from 31.7 to 19.3 m^3.

Fast-ion-driven modes, such as toroidal Alfvén eigenmodes (TAEs), have been observed in most stellarators. Such modes arise in the gaps of the continuous Alfvén spectrum that form when a plasma cylinder is bent into a torus. In stellarators, the breaking of axisymmetry gives rise to additional gaps and discrete modes lying therein. There are therefore more types of Alfvén eigenmodes in stellarators than in tokamaks, e.g. helicity- and mirror-induced Alfvén eigenmodes, there are more wave–particle resonances, and thus more scope for instability [17]. For instance, while in a circular tokamak with large aspect ratio the main TAE resonances are $v_\parallel = v_\mathrm{A}$ and $v_\parallel = v_\mathrm{A}/3$, where v_A is the Alfvén speed, it is possible to have resonances with $v_\parallel > v_\mathrm{A}$ in stellarator geometry. On the other hand, the alpha-particle pressure in a reactor is proportional to the slowing-down time,

$$p_\alpha \sim \tau_\mathrm{s} \sim T_\mathrm{e}^{3/2}/n_\mathrm{e},$$

which is expected to be smaller in stellarators than in tokamaks, thanks to the ability of the former to operate above the Greenwald limit. The fast-particle drive for Alfvénic modes can thus be smaller in the stellarator, if an operating point with high density can be chosen. Note that at constant thermal pressure, $p \sim n_\mathrm{e}T_\mathrm{e}$ or fusion power $P_\mathrm{fus} \sim n_\mathrm{e}^2 T_\mathrm{i}^2$, the alpha-particle pressure scales as $p_\alpha \sim n_\mathrm{e}^{-5/2}$, so increasing the plasma density by a factor of 2.5 leads to ten times lower alpha-particle pressure.

3.1. More mathematical issues

45 years ago, Grad [18] pointed out that general scalar-pressure MHD equilibria are likely to be very complicated when the plasma is not axisymmetric. Unless awkward conditions are satisfied, the pressure gradient must vanish on every rational surface, and flux surfaces will not exist throughout the plasma in general. Toroidal magnetic fields without a continuous symmetry are composed of a fractal mix of chaotic field lines, magnetic islands and intact flux surfaces. It has been argued that the only nontrivial solutions to the equation $\boldsymbol{J}\times\boldsymbol{B} = \nabla p$ in chaotic regions contain an uncountable infinity of discontinuities in both ∇p and $\boldsymbol{J}$, and on these grounds fundamental criticism can be raised against codes that attempt to solve this equation numerically [19].

There appear to be three ways out of this dilemma. The most common one is the method chosen by the VMEC code [20], which insists on the existence of nested flux surfaces and computes the equilibrium by minimizing the MHD energy subject to the mathematical constraints that follow. In general, there will then be an infinite Pfirsch–Schlüter current density on most rational surfaces, diverging as $1/x$ with the distance x from the surface. (Alternatively, the pressure gradient could vanish on all rational surfaces). In practice, however, the numerical resolution is usually sufficiently limited that most of these singularities are not noticeable.

The second way is to allow magnetic surfaces to break up and form islands and stochastic regions, but to ignore the infinity of singularities that these imply, e.g. by letting them be washed out by finite spatial resolution. Physically, this might be justified by arguing that the MHD equilibrium condition $\boldsymbol{J}\times\boldsymbol{B} = \nabla p$ is modified by kinetic effects (leading to finite viscosity and flow) on small scales.

Finally, one can insist on solving orthodox force balance, $\boldsymbol{J}\times\boldsymbol{B} = \nabla p$, implying $\boldsymbol{B}\cdot\nabla p = 0$, so that the pressure vanishes exactly in chaotic regions. Dewar, Hudson and co-workers have shown that it is possible to make the problem tractable by taking the pressure profile to be 'stepped'. That is, the pressure is prescribed to be piecewise constant and to change discontinuously at a finite number of irrational flux surfaces, between which the field is assumed to be in a Taylor-relaxed state. The mathematical problem of finding such an equilibrium can be formulated as a variational principle suitable for numerical solution, see [21] and papers cited therein.

Mathematical subtleties specific to non-axisymmetric plasmas also arise in the theory of ballooning modes [22]. The ballooning equation predicts different stability properties for different field lines on the same flux surface in a stellarator, and it is not straightforward to construct global modes, since the solutions to the ray equations generally are chaotic. There are parallels to the semi-classical theory of quantum systems with chaos [23].

4. Neoclassical transport

The advantages of stellarators discussed above—steady state, high density, the absence of current-driven instabilities and disruptions—come not only at the price of complicated geometry. As Gibson and Taylor observed [24], there are generally unconfined particle orbits regardless of the magnetic-field strength. This is not only problematic for the confinement

of alpha particles, whose orbits are practically collisionless, but can also lead to prohibitively high neoclassical transport of the thermal particle species.

4.1. Typical collisionality regimes

There are several different collisionality regimes for neoclassical transport in stellarators, and in contrast to the situation in tokamaks the electrons and ions are often in different regimes. These have been reviewed in great detail elsewhere [25–29], and it has been established that the neoclassical heat flux is very significant in the plasma core of most experiments. At low collisionality, the electrons are usually in the $1/\nu$-regime, where the diffusivity is inversely proportional to the collision frequency ν,

$$D_e \sim \frac{\epsilon_{\rm eff}^{3/2} v_d^2}{\nu_e}, \qquad (2)$$

and thus scales as

$$D_e \propto \frac{\epsilon_{\rm eff}^{3/2} T_e^{7/2}}{n_e B^2 R^2}.$$

Here $\epsilon_{\rm eff}$ is a geometric quantity characterizing the confinement qualities of trapped-particle orbits, v_d is their drift velocity, T_e is the electron temperature and R is the major radius of the device. Because of the strong T_e scaling, the neoclassical losses are expected to dominate at high electron temperature, and this is indeed observed to be the case. In W7-AS, the transport followed neoclassical predictions in roughly half the plasma volume if the temperature was high enough ($\gtrsim$1 keV) and was attributed to turbulence in the outer regions of the plasma [11].

The scaling (2) has a simple origin. In a classical stellarator, the particles responsible for the transport are trapped in local magnetic wells of depth $\delta B/B \sim \epsilon_h$, the helical magnetic ripple, and drift radially at the velocity v_d. Collisions scatter the particles in and out of the wells on the time scale of the inverse effective collision frequency, $\Delta t \sim 1/\nu_{\rm eff} \sim \epsilon_h/\nu$. They therefore undergo a random walk with step size $\Delta r = v_d \Delta t$, and the diffusion coefficient (2) results from multiplying the estimate $\Delta r^2/\Delta t$ by the fraction of locally trapped particles $\epsilon_h^{1/2}$ (taking $\epsilon_{\rm eff} \sim \epsilon_h$). In stellarators that have been optimized for low neoclassical transport, the trapped particles have reduced radial drift velocities, and the parameter $\epsilon_{\rm eff}$ in equation (2) is substantially smaller than the fraction of trapped particles, see figure 3.

If the collisionality is so low that the step size Δr becomes comparable to the radial scale length, the transport is no longer radially local [30]. This is a qualitative difference to the tokamak, where the neoclassical random-walk step size is always limited from above by the banana width, so that, as long as the latter is thinner than the gradient length scale, the transport is always local in nature.

The diffusion coefficient (2) is much larger for ions than for electrons and would therefore violate ambipolarity. An inward-pointing radial electric field therefore arises and serves to confine the ions and reduce their transport to the electron level (whilst increasing the electron transport somewhat). The

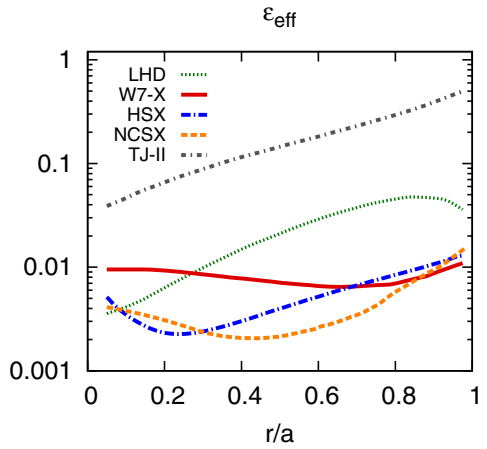

Figure 3. Neoclassical confinement quality parameter $\epsilon_{\rm eff}$ versus minor radius in various stellarators: TJ-II, LHD ($R_0 = 3.60$ m configuration), W7-X (standard configuration), NCSX and HSX.

way this happens is that the electric field gives rise to a poloidal $\boldsymbol{E} \times \boldsymbol{B}$ drift that prevents the locally trapped ion orbits from drifting all the way to the wall. Instead, the radial excursion of the bounce-averaged ion orbits becomes of order $\Delta r \sim v_d/\Omega_E$, where $\Omega_E \sim E_r/rB$ is the frequency of the poloidal drift. In the absence of collisions, these orbits are thus confined (if $\Delta r < r$), but will undergo a random walk with the step size Δr when collisions are present and scatter the particles in and out of the local trapping regions. The effective collision frequency for such scattering depends quadratically on the distance $\Delta\xi$ (in terms of pitch angle) to the trapping boundary in velocity space, $\nu_{\rm eff} \sim \nu/\Delta\xi^2$. Multiplying $\nu_{\rm eff}\Delta r^2$ by the fraction of participating particles ($\sim\Delta\xi$) gives the diffusion coefficient estimate

$$D_i \sim \frac{\nu}{\Delta\xi}\left(\frac{v_d}{\Omega_E}\right)^2,$$

which diverges as $\Delta\xi \to 0$, indicating that the most important role is played by particles close to the trapping boundary. The width of this boundary layer is limited from below by the requirement $\nu_{\rm eff} \lesssim \Omega_E$, which implies $\Delta\xi \gtrsim (\nu/\Omega_E)^{1/2}$ and results in the diffusion coefficient

$$D_i \sim \frac{\nu^{1/2} v_d^2}{\Omega_E^{3/2}}$$

in what is, accordingly, called the $\sqrt{\nu}$-regime.

When a shallowly trapped ion orbit is convected poloidally by the $\boldsymbol{E} \times \boldsymbol{B}$ drift into a region of lower magnetic mirror ratio, it will undergo collisionless detrapping, and when it is convected back into the region with higher mirror ratio, it will again ultimately become trapped. The collisional scattering of ions with such orbits results in a random walk with a diffusion coefficient proportional to the collision frequency, so that the $\sqrt{\nu}$-regime metamorphoses into a ν-regime at low collisionality.

This situation, with a negative radial electric field, the electrons in the $1/\nu$-regime (2) and the ions in the $\sqrt{\nu}$-regime (or ν-regime), is typical but does not always apply. The ambipolarity equation (electron flux = ion flux) determining

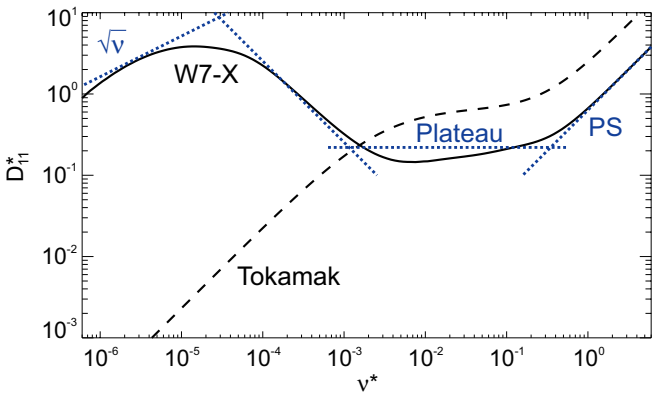

Figure 4. The so-called 'mono-energetic' diffusion coefficient (see [29] for details) versus collisionality, $\nu^* = \nu R/\iota v$, where ν is the mono-energetic pitch-angle-scattering frequency, R is the major radius and v is the speed of the particles, in the standard configuration of W7-X (bold) and a tokamak (dashed) with similar aspect ratio ($r/R = 0.255/5.527$) and an elongation of 1.5. The asymptotic regimes are indicated by dotted straight lines. In the order of increasing collisionality: the $\sqrt{\nu}$-regime, the $1/\nu$-regime, the plateau regime and the Pfirsch–Schlüter regime. At very low collisionality (below the range shown) the transport again becomes proportional to ν. The diffusivity has been normalized to the plateau value in a circular tokamak, and the radial electric field has been chosen as $E_r/vB = 3 \times 10^{-5}$, where B is the magnetic-field strength.

the radial electric field is highly nonlinear and generally has three roots for the electric field. The 'ion root' corresponds to the scenario just described, one root is always unstable, and the 'electron root', with $E_r > 0$, is typically realized when the electrons are subject to strong and localized heating. Finally, it should be mentioned that there are also other collisionality regimes, and that the different regimes are not always well separated from each other. In practice, therefore, it is usually necessary to calculate the neoclassical transport numerically [29]. Figure 4 shows the typical result of such a calculation, with the different regimes indicated by straight lines.

4.2. Plasma rotation

All of this is very different from axisymmetric devices, where the neoclassical transport is usually small and intrinsically ambipolar in lowest order. The physics of plasma rotation is therefore qualitatively different in tokamaks and stellarators. An axisymmetric plasma is essentially free to rotate as it pleases. The angular momentum is a conserved quantity, just like mass and energy, and can only change because it is transported radially. The rotation profile is determined by this transport and by the sources (NBI) and sinks (friction against neutral atoms) of angular momentum, and the relaxation towards a steady-state rotation profile occurs on the confinement time scale. The toroidal rotation velocity frequently reaches a considerable fraction of the ion thermal speed, v_{T_i}, even in the absence of deliberate momentum sources.

In stellarators, however, it follows immediately from the drift-kinetic equation that such fast rotation is generally impossible [31]. In fact, this conclusion is reached already *in zeroth order* of the gyroradius expansion and is therefore independent of any turbulent fluctuations, regardless of their nature, as long as they are small. Moreover, plasma rotation turns out to be impeded even in quasisymmetric stellarators [32, 33].

Proceeding to the next order in $\rho_* = \rho_i/L$, where ρ_i is the ion gyroradius and L is the macroscopic length, one may ask what governs plasma rotation comparable to the diamagnetic velocity $V \sim \rho_* v_{T_i}$. Again, the situation is very different in stellarators and in tokamaks. In stellarators, the rotation is set by the requirement that the transport should be ambipolar. Because the turbulent transport is automatically ambipolar in the gyrokinetic approximation [34], regardless of the magnetic geometry and of whether the transport is electrostatic or electromagnetic, it is the neoclassical transport that determines the radial electric field on length scales exceeding the gyroradius [35]. Zonal flows are still possible, but have qualitatively different characteristics from those in tokamaks [36, 37]. In tokamaks, the neoclassical transport is automatically ambipolar, so one must proceed yet one order higher in the ρ_*-expansion, where the rotation is set by neoclassical and turbulent momentum transport. An exception occurs if the axisymmetry is broken by error fields. The neoclassical transport then becomes non-ambipolar and sets the rotation—a phenomenon somewhat misleadingly referred to as neoclassical toroidal viscosity.

4.3. Quasisymmetric and quasi-isodynamic stellarators

Nearly all the differences between stellarators and tokamaks concerning neoclassical transport disappear in one important limit, namely, when the stellarator is exactly quasi-axisymmetric [38] or quasi-helically symmetric [39, 40]. There are a number of equivalent mathematical definitions of these concepts, e.g.

- $B(\psi, \theta, \varphi) = |\boldsymbol{B}|$ should be expressible as a function of the flux-surface label ψ and a single helicity angle, $m\theta - n\varphi$, where m and n are integers, and (θ, φ) are Boozer or Hamada angles;
- $[(\boldsymbol{B} \times \nabla\psi) \cdot \nabla B]/(\boldsymbol{B} \cdot \nabla B)$ should depend only on ψ;
- $\boldsymbol{B} \cdot \nabla B$ should be a function only of ψ and B;
- B should be a periodic function of the arc length on each flux surface, $B(\psi, l + L(\psi)) = B(\psi, l)$.

Each of these statements is equivalent to all the others if the rotational transform is irrational and the flow is small, $V \sim \rho_* v_{T_i}$, and they all then imply that the usual drift-kinetic equation is isomorphic to that in a tokamak [41]. The neoclassical transport properties are therefore similar to lowest order in ρ_*. Thus, in the exactly quasisymmetric limit, there are no regimes of $1/\nu$- or $\sqrt{\nu}$-transport, and the neoclassical transport is intrinsically ambipolar. The transport coefficients are numerically different from those in a tokamak—the bootstrap current can for instance be negative—but they do not need to be calculated anew; there is a simple recipe for converting them between axisymmetric and quasisymmetric configurations [41, 43]. However, it is not possible to achieve *exact* quasisymmetry [42], and a small violation of the symmetry can sometimes lead to substantially

enhanced transport. For instance, all stellarator designs have a clear $1/\nu$-regime, even those that have been optimized to be quasisymmetric, but the coefficient in front of this scaling can be made to be much smaller than in a classical stellarator [29].

Unlike quasi-axisymmetry and quasi-helical symmetry, it is not possible to achieve quasi-poloidal symmetry to any particularly high degree of approximation, at least not in the vicinity of the magnetic axis, where the pressure gradient vanishes in the expression

$$\boldsymbol{\kappa} = \frac{\mu_0 \nabla p}{B^2} + \frac{\nabla_\perp B}{B},$$

implying that the magnetic-field strength increases in the direction of the curvature vector $\boldsymbol{\kappa}$ and therefore cannot be independent of the poloidal angle θ.

Whilst quasisymmetry makes a stellarator as similar as possible to a tokamak, in some sense, it is not a necessary condition for achieving good neoclassical confinement. Mathematically, what is required is that the parallel adiabatic invariant,

$$J = \int m v_\parallel \, \mathrm{d}l,$$

should be (approximately) constant on flux surfaces for all trapped orbits, where the integral is taken along the field between two consecutive bounce points. Differentiation of J at constant energy and magnetic moment gives the bounce-averaged drift

$$\overline{\dot{\psi}} = \frac{1}{Ze\tau_\mathrm{b}} \frac{\partial J}{\partial \alpha}, \tag{3}$$

$$\overline{\dot{\alpha}} = -\frac{1}{Ze\tau_\mathrm{b}} \frac{\partial J}{\partial \psi}, \tag{4}$$

where τ_b is the bounce time, Ze is the charge, the magnetic field has been written as $\boldsymbol{B} = \nabla\psi \times \nabla\alpha$, and an overbar denotes the bounce average. Here ψ measures the toroidal flux and $\alpha = \theta - \iota\varphi$ labels the different field lines on each flux surface. A configuration with vanishing bounce-averaged drift, $\partial J/\partial\alpha = 0$, is called omnigenous [44], and if the contours of constant magnetic-field strength are poloidally, but not toroidally, closed one speaks of quasi-isodynamic configurations [45, 46]. W7-X is the first stellarator to approach quasi-isodynamicity (close to the axis at high beta) but substantially more quasi-isodynamic designs have been found in recent years [47], although exact quasi-isodynamicity is impossible to achieve [48]. Whereas the neoclassical transport coefficients generally have to be calculated numerically in most stellarators, the exactly omnigenous or quasi-isodynamic limit is amenable to analytical treatment [49].

The bootstrap current is positive in quasi-axisymmetric stellarators, negative in quasi-helically symmetric ones, and is close to zero in quasi-isodynamic devices [29, 50, 51]. The latter have the additional property that the Pfirsch–Schlüter current closes within each period of the configuration [47]. This property follows from the fact that the streamlines of the current are tangential to the level curves of maximum magnetic-field strength, and therefore close poloidally. Quasi-isodynamic stellarators therefore have small Shafranov shift.

4.4. Particle transport

When stellarators are optimized for low neoclassical transport the goal is, of course, to bring it down to a level comparable to (or below) that expected from the turbulence. Because of the strong temperature scaling in the $1/\nu$-regime, neoclassical transport tends to dominate in the centre of the plasma, and sometimes in almost the entire plasma volume [52]. But even if the magnitude of the neoclassical transport has been reduced to an acceptable level, it may nevertheless cause problems concerning particle confinement.

The neoclassical particle flux of each species a is of the form

$$\langle \boldsymbol{\Gamma}_a \cdot \nabla r \rangle = -n_a \sum_b \left[D_1^{ab} \left(\frac{\mathrm{d}\ln n_b}{\mathrm{d}r} + \frac{e_b}{T_b} \frac{\mathrm{d}\phi}{\mathrm{d}r} \right) + D_2^{ab} \frac{\mathrm{d}\ln T_b}{\mathrm{d}r} \right], \tag{5}$$

where r is an arbitrary flux-surface label and the sum is taken over all the species b present in the plasma. The terms with $b \neq a$ are due to the friction along $\boldsymbol{B}$ between the different species and are in stellarators negligible in comparison with the $b = a$ term at low collisionality. In contrast to tokamaks, the radial electric field, $E_r = -\mathrm{d}\phi/\mathrm{d}r$, enters as a thermodynamic force. As already mentioned, E_r is determined by the requirement of ambipolarity and is negative under the usual ion-root conditions. For heavy impurities, whose charge $e_a = Ze$ is large, the electric field thus tends to cause impurity accumulation. This is a stronger effect than neoclassical impurity accumulation in tokamaks, which is caused by the friction force between bulk ions and impurities and leads to an inward flux of the *latter* at a rate proportional to the density and temperature gradients of the *former* [53].

The second potential problem caused by neoclassical particle transport has to do with the fact that, in all stellarator collisionality regimes, D_2^{ab} is positive, so that the temperature gradient in equation (5) causes outward particle flux and thus tends to create a hollow density profile [54]. Such profiles have been observed on LHD and may necessitate central particle fuelling in a reactor.

It may be possible to solve both these problems by making the magnetic field approximately quasi-isodynamic, so that the outward thermodiffusion and the radial electric field are very small [55]. Very good collisionless particle-orbit confinement is also necessary for confining fast ions. W7-X enjoys good fast-particle confinement only at high beta and close to the magnetic axis.

5. Microinstabilities and turbulence

5.1. Analytical considerations

Although the neoclassical transport is much larger than in tokamaks, turbulence also contributes significantly to the transport in stellarators, particularly in cooler parts of the plasma, where $1/\nu$-transport does not occur. The study of stellarator microinstabilities is, however, still in its infancy, and there is not much in the way of analytical theory in the literature. In a generic stellarator, one expects broadly the same microinstabilities to be present as in a tokamak, but

their strength can be different, and the freedom to design the magnetic field appropriately may make it possible to reduce their growth rates [56].

To keep the discussion as simple as possible, we restrict our attention to collisionless instabilities in the electrostatic approximation. (For a general background to the mathematical apparatus in the tokamak context, see, e.g. [57]). We adopt the ballooning representation [22], writing for each perturbation

$$\phi(\psi,\theta,\varphi)=\sum_{k=-\infty}^{\infty}\tilde{\phi}(\psi,\theta-2\pi k,\varphi), \tag{6}$$

which automatically ensures periodicity in θ, whatever the choice of the function $\tilde{\phi}$, and we write

$$\tilde{\phi}(\psi,\theta,\varphi)=\hat{\phi}(\psi,\theta,\varphi)\mathrm{e}^{\mathrm{i}S(\psi,\alpha)}, \tag{7}$$

where $\hat{\phi}$ varies slowly in all directions and S is constant along the magnetic field but varies rapidly across it. The functions $\hat{\phi}(\psi,\theta,\varphi)$ and $\mathrm{e}^{\mathrm{i}S(\psi,\alpha)}=\mathrm{e}^{\mathrm{i}S(\psi,\theta-\iota\varphi)}$ need not be periodic in θ but are supposed to be 2π-periodic in φ, so that $\phi(\psi,\theta,\varphi)$ also acquires this periodicity. The wave vector is $\boldsymbol{k}_\perp=k_\psi\nabla\psi+k_\alpha\nabla\alpha$, where $k_\psi=\partial S/\partial\psi$ and $k_\alpha=\partial S/\partial\alpha$.

The gyrokinetic equation for the non-adiabatic part of the distribution function of each species, $g_a=f_{a1}+(e_a\phi/T_a)f_{a0}$, now becomes

$$\mathrm{i}v_\parallel\nabla_\parallel\hat{g}_a+(\omega-\omega_{\mathrm{d}a})\hat{g}_a=\frac{e_a\hat{\phi}}{T_a}J_0(k_\perp v_\perp/\Omega_a)\left(\omega-\omega_{*a}^T\right)f_{a0},$$

where $\omega_{\mathrm{d}a}=\boldsymbol{k}_\perp\cdot\boldsymbol{v}_{\mathrm{d}a}$ denotes the drift frequency and $\omega_{*a}^T=\omega_{*a}[1+\eta_a(x^2-3/2)]$, with $\omega_{*a}=(T_ak_\alpha/n_ae_a)\mathrm{d}n_a/\mathrm{d}\psi$, $\eta_a=\mathrm{d}\ln T_a/\mathrm{d}\ln n_a$, $\Omega_a=e_aB/m_a$ and $x^2=m_av^2/2T_a$. The system is closed by the quasineutrality condition

$$\sum_a\frac{n_ae_a^2}{T_a}\hat{\phi}=\sum_a e_a\int\hat{g}_aJ_0\mathrm{d}^3v. \tag{8}$$

In the usual drift-wave ordering,

$$k_\parallel v_{T_\mathrm{i}}\ll\omega\ll k_\parallel v_{T_\mathrm{e}}, \tag{9}$$

$$k_\perp\rho_\mathrm{e}\ll k_\perp\rho_\mathrm{i}\sim O(1),$$

it is straightforward to solve the gyrokinetic equation for ions and trapped electrons, respectively,

$$\hat{g}_\mathrm{i}=\frac{\omega-\omega_{*\mathrm{i}}^T}{\omega-\omega_{\mathrm{di}}}\frac{eJ_0\hat{\phi}}{T_\mathrm{i}}f_{\mathrm{i}0}, \tag{10}$$

$$\hat{g}_\mathrm{e}^{\mathrm{tr}}=-\frac{\omega-\omega_{*\mathrm{e}}^T}{\omega-\overline{\omega}_{\mathrm{de}}}\frac{e\overline{\hat{\phi}}}{T_\mathrm{e}}f_{\mathrm{e}0}, \tag{11}$$

where an overbar again denotes the bounce average. For circulating electrons the non-adiabatic response is a factor $\omega/k_\parallel v_{T_\mathrm{e}}$ smaller than $\hat{g}_\mathrm{e}^{\mathrm{tr}}$ and will be neglected.

The purely curvature-driven ion-temperature-gradient (ITG) mode results from making these approximations and, additionally, neglecting the non-adiabatic electron response altogether, i.e. setting $g_\mathrm{e}=0$. The dispersion relation obtained from equations (8) and (10) is then identical to that in a tokamak with the same local drift frequency ω_{di}, and has been treated, e.g., in [58]. Because of the locality assumption, $k_\parallel v_{T_\mathrm{i}}\ll\omega$, there is no difference between a tokamak and a stellarator with the same local radius of curvature of the magnetic field. However, the validity of the approximation is more restricted in stellarators, because the connection length along $\boldsymbol{B}$ between regions with different physical conditions tends to be shorter. In the tokamak, this length is of order $qR=R/\iota$ whereas in stellarators it is rather the toroidal extent of one period of the device. One therefore expects ITG modes to be less curvature-driven and more slab-like—an expectation that is indeed borne out in numerical simulations.

Collisionless trapped-electron modes (TEMs) are obtained by retaining the response (11), in particular the resonance in the denominator. The simplest description is obtained by treating the trapped-particle fraction as small and neglecting the magnetic drift frequency by taking $\omega_{\mathrm{di}}/\omega\ll1$ [59]. Thus, in leading order inserting

$$\hat{g}_\mathrm{i}=\left(1-\frac{\omega_{*\mathrm{i}}^T}{\omega}\right)\frac{eJ_0\hat{\phi}}{T_\mathrm{i}}f_{\mathrm{i}0},$$

and $g_\mathrm{e}=0$ in equation (8) gives the drift-wave dispersion relation

$$\frac{\omega}{\omega_{*\mathrm{e}}}=\frac{\Gamma_0+\eta_\mathrm{i}(\Gamma_1-\Gamma_0)}{\tau(1-\Gamma_0)+1}, \tag{12}$$

where $\tau=T_\mathrm{e}/T_\mathrm{i}$, $\Gamma_n=I_n(b)\mathrm{e}^{-b}$, I_n is a modified Bessel function and $b=k_\perp^2T_\mathrm{i}/(m_\mathrm{i}\Omega_\mathrm{i}^2)$. The asymptotic forms are [60]

$$\omega\simeq\omega_{*\mathrm{e}},\qquad b\ll1,$$

$$\frac{\omega}{\omega_{*\mathrm{e}}}\simeq\frac{1-\eta_\mathrm{i}/2}{(1+\tau)\sqrt{2\pi b}},\qquad b\gg1,$$

and one finds numerically from equation (12) that $\omega/\omega_{*\mathrm{e}}$ is always positive if $0<\eta_\mathrm{i}<1.64$, so that the drift wave then propagates in the electron diamagnetic direction for all wave numbers. Its stability is determined in the next order of our expansion in the number of trapped particles, where the denominator in the electron response (11) provides the possibility of a resonant drive. But this resonance, $\omega=\overline{\omega}_{\mathrm{de}}$, only exists if $\omega_{*\mathrm{e}}\overline{\omega}_{\mathrm{de}}>0$ (assuming $\eta_\mathrm{i}<1.64$), so that the electrons precess in the same direction that drift waves propagate. For modes with $k_\psi=0$, or in omnigenous configurations, where according to equation (4)

$$\overline{\omega}_{\mathrm{de}}=k_\alpha\overline{\boldsymbol{v}_{\mathrm{de}}\cdot\nabla\alpha}=\frac{k_\alpha}{e\tau_b}\frac{\partial J}{\partial\psi},$$

this requires

$$\omega_{*\mathrm{e}}\overline{\omega}_{\mathrm{de}}=-\frac{k_\alpha^2T_\mathrm{e}}{n_\mathrm{e}e^2\tau_b}\frac{\partial J}{\partial\psi}\frac{\mathrm{d}n_\mathrm{e}}{\mathrm{d}\psi}>0.$$

In *maximum-J* configurations, i.e. where $\partial J/\partial\psi<0$, one does thus not expect collisionless TEMs, at least not in their usual guise. (Any instability would have to be driven by a resonance with the ions or subthermal electrons with $v_\parallel\sim\omega/k_\parallel\ll v_{T_\mathrm{e}}$.) Physically, the requirement $\partial J/\partial\psi<0$ means that the bounce-averaged curvature is favourable, which according

to equation (4) leads to reversal of the precessional drift. In tokamaks, this requirement is met by trapped particles whose bounce points lie sufficiently far into the inboard side of the torus that the particles spend most of their time in the good-curvature region. But deeply trapped particles have positive $\partial J/\partial\psi$ in a typical tokamak, reflecting the circumstance that the bad-curvature region coincides with the trapping region. This need not be the case in stellarators, and, indeed, perfectly quasi-isodynamic stellarators are maximum-J devices. As we have just seen, the simplest form of the TEM is not present in such configurations, and in [61] it is shown from basic energy considerations that any particle species with $k_\parallel v_{Ta} \gg \omega$ and $0 < \eta_a < 2/3$ exerts a stabilizing influence on arbitrary electrostatic, collisionless instabilities. Physically, the point is that, because J is an adiabatic invariant, if an instability with $\omega\tau_b \ll 1$ results in the radial movement $\Delta\psi$ of a particle, then

$$\Delta J = \frac{\partial J}{\partial \psi}\Delta\psi + \frac{\partial J}{\partial E}\Delta E = 0,$$

where E is the kinetic energy and $\partial J/\partial E > 0$. The particle must therefore gain an amount of energy equal to

$$\Delta E = -\frac{\partial J/\partial\psi}{\partial J/\partial E}\,\Delta\psi,$$

at the expense of the instability in question. The condition $\partial J/\partial\psi < 0$ thus promotes stability if $\mathrm{d}n/\mathrm{d}\psi < 0$.

We are thus led to the conclusion that density-gradient-driven TEMs should be stable within the usual ordering (9), whose limitations should, however, not be forgotten. Since $\omega \sim \omega_{*\mathrm{e}} \sim k_\perp \rho_\mathrm{i} v_{T_\mathrm{i}}/L_n$, where L_n is the length scale of the radial density profile, we have

$$\frac{\omega}{k_\parallel v_{T_\mathrm{e}}} \sim \frac{k_\perp \rho_\mathrm{i}}{k_\parallel L_n}\sqrt{\frac{m_\mathrm{e}}{m_\mathrm{i}}}.$$

If the density gradient or the parallel wavelength is sufficiently large, this quantity will not be much smaller than unity and the ordering (9) will be violated.

5.2. Gyrokinetic simulations

Only relatively recently have gyrokinetic codes for stellarator geometry become available [62–66], and not enough information has accumulated from these to say anything definite about the turbulence properties of various configurations. Most of the codes operate in flux-tube geometry or have only very recently become able to treat an entire flux surface, and others only solve the linear gyrokinetic equation. Nearly all the simulations have been made in the electrostatic approximation, most of them with adiabatic electrons, and none have (to our knowledge) included collisions. Nevertheless, from those simulations that have been carried out, some important differences between stellarators and tokamaks appear to be emerging.

The EUTERPE code [62] has in recent months performed the first global and electromagnetic, but linear, gyrokinetic simulations of a stellarator, and preliminary results are shown in figure 5. These simulations treat both the ions and the electrons kinetically, with the correct mass ratio, and the geometry is that of the high-mirror configuration of

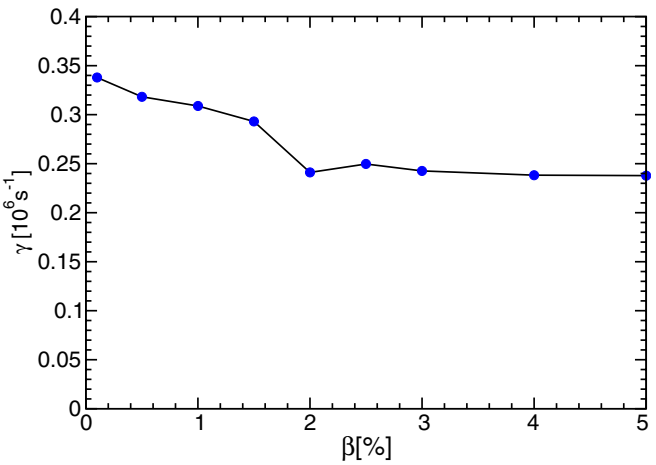

Figure 5. Growth rate of the fastest-growing mode versus $\langle\beta\rangle$ in Wendelstein 7-X, calculated by the global, electromagnetic, gyrokinetic code EUTERPE. Unlike the typical situation in a tokamak, there is no sign of rapidly growing kinetic ballooning modes at high $\langle\beta\rangle$.

Wendelstein 7-X, with constant density, electron temperature $T_\mathrm{e} = 8.2\,\mathrm{keV}$, and an ion temperature profile given by

$$\ln\frac{T_\mathrm{i}(s)}{T_\mathrm{i}(s_0)} = -\frac{\kappa_T}{1-\mathrm{sech}^2\frac{s_0}{w}} \times\left[w\tanh\left(\frac{s-s_0}{w}\right) - (s-s_0)\mathrm{sech}^2\frac{s_0}{w}\right],$$

where $s \in [0,1]$ is the normalized toroidal flux, $\kappa_T = 3.5$, $s_0 = 0.5$, $w = 0.3$, and $T_\mathrm{i}(s_0) = 8.2\,\mathrm{keV}$. The code solves an initial-value problem, and figure 5 shows the growth rate of the resulting fastest-growing linear mode in the system. As in tokamaks, the growth rate is seen to drop with increasing beta, but unlike the situation in a typical tokamak this trend continues all the way to $\langle\beta\rangle = 5\%$ and is not interrupted by the growth of kinetic ballooning modes, presumably because the device has been optimized for good ideal-MHD stability and the ideal-MHD ballooning threshold is considerably higher than in most tokamaks. As $\langle\beta\rangle$ increases, the equilibrium changes because of plasma diamagnetism in the direction of becoming more quasi-isodynamic, which would have a stabilizing effect on microinstability even if the electromagnetic terms were ignored in the gyrokinetic equation.

The GENE and GS2 codes were both originally developed to operate in tokamak flux-tube geometry, but have later been extended to be able to treat stellarator flux tubes [64, 66]. GS2 found the linear threshold for ITG modes with adiabatic electrons in NSCX to be $a/L_{T_\mathrm{i}} \simeq$ 1–2, where a is the minor radius and L_{T_i} the ITG scale length, and electrostatic simulations with kinetic electrons also found density-gradient-driven TEMs, in agreement with earlier simulations using the FULL code [63].

The stellarator version of GENE has now been developed a step further so that it can make simulations of an entire flux surface (or, more commonly, of one period thereof) but still makes a local approximation in the radial direction. The Japanese GKV code has undergone a similar extension [67], which appears necessary since, in stellarators, different flux

tubes (of finite length) on the same flux surface can have different microinstability properties. The most unstable flux tube in a stellarator is usually the one that crosses the outboard midplane in one of the up–down symmetric poloidal cross sections, in W7-X and NCSX in the bean-shaped cross section. From the full-surface version of GENE, it appears that the flux surface as a whole is somewhat more stable than the most unstable flux tube: the latter may support a locally growing mode even though the flux surface as a whole is linearly stable. On the other hand, from nonlinear simulations of ITG modes with adiabatic electrons it appears that turbulence may still be present in such situations. That is, stellarator-specific 'subcritical' turbulence may be present if the gradients are chosen in the interval where some flux tubes are locally unstable but the flux surface as a whole is not.

The mode structure of microinstabilities depends on the magnetic-field geometry and is thus different in tokamaks and stellarators [68–70]. In both types of devices, the curvature is usually most unfavourable on the outboard side of the device, and the turbulent fluctuations are observed to peak there, see figure 6. However, the local magnetic shear tends to be much larger in stellarators and serves to localize the fluctuations; in fluid simulations of W7-X a sudden drop in fluctuation amplitude is observed where a magnetic field line crosses the 'helical edge' [71]. In the context of a GENE simulation with adiabatic electrons, this effect is further illustrated by figure 7, which shows level curves of root-mean-squared potential fluctuations as functions of the poloidal and toroidal Boozer angles. These structures are elongated along the magnetic field, but substantially less so than in a typical tokamak. Instead of extending all the way around the torus, each one of them is limited to about one period of the device. In the figure, level curves of $|\nabla\alpha|^2$ are also shown, and it appears that the turbulence shuns regions where this quantity is large, i.e. where the flux tubes are strongly compressed in the direction of $\nabla\alpha$.

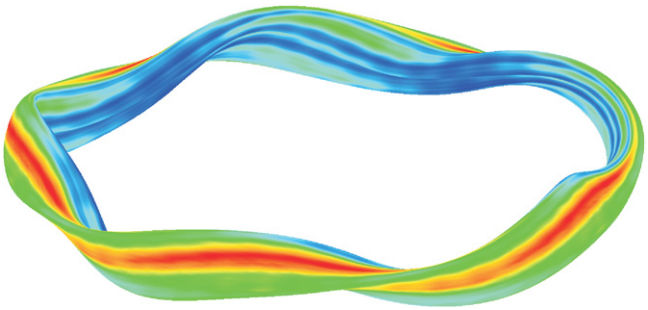

Figure 6. Root-mean-squared electrostatic potential on a W7-X flux surface in GENE simulations of ITGs with adiabatic electrons in W7-X. The turbulence peaks on the outboard side, where the magnetic-field curvature is unfavourable, and the fluctuations extend for about one period along the magnetic field.

Most stellarators have negative (or very small) global magnetic shear according to the tokamak definition, $q' = -\iota'/\iota^2 < 0$, which tends to be stabilizing for curvature-driven modes. That this is the case also in stellarators was observed in nonlinear fluid turbulence simulations by Kleiber and Scott [71]. Antonsen *et al* [72] suggested a physical mechanism based on the poloidal tilting of turbulent eddies induced by the magnetic shear, and figure 8 shows evidence of this phenomenon. As seen in the figure, the eddies are horizontal at $\alpha = 0$, which corresponds to the outboard midplane in the bean-shaped cross section and 'fan out' from this region in the manner envisaged by Antonsen *et al*. Similar observations have been made in simulations of tokamaks with negative magnetic shear [73].

In summary, it is too early to say whether gyrokinetic turbulence is more benign in stellarators than in tokamaks. It appears that stellarators should benefit from their negative global magnetic shear, their large local shear (which assumes both positive and negative values, and peaks where the flux surface is strongly bent), and the fact that trapping regions do not necessarily overlap with regions of bad curvature. On the other hand, they suffer from a larger area-to-volume ratio and from zonal-flow damping through electron collisions because of non-ambipolar neoclassical transport.

6. Edge and divertor physics

The differences between tokamak and stellarator divertor physics have recently been reviewed by Feng *et al* [74], and will therefore only be outlined briefly here. Only two stellarators,

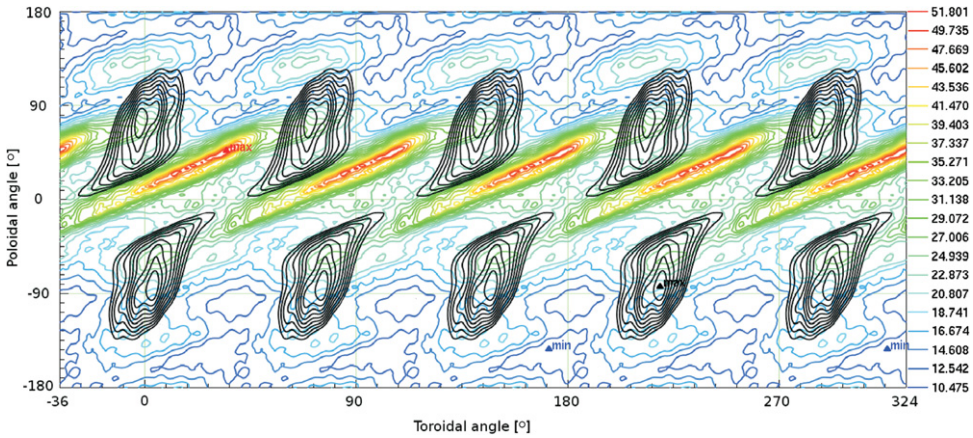

Figure 7. The same quantity as in figure 6 as a function of the toroidal and poloidal Boozer angles. Also plotted (in black) are level curves of $|\nabla\alpha|^2$, from which it appears that the turbulence does not penetrate into regions where this quantity is large.

W7-AS and LHD, have operated with proper divertors, and these are geometrically very different from each other. LHD has a helical divertor with a partially stochastic magnetic field, whereas W7-AS used the naturally occurring chain of magnetic islands beyond the last closed flux surface to divert the escaping plasma to divertor plates, see figure 9. W7-X is also being built with an island divertor based on this concept, which makes the connection length to the target an order of magnitude longer than in similarly shaped tokamaks. In the latter, the magnetic field is diverted by a poloidal field of comparable magnitude to that produced by the plasma current, $B_\theta/B \sim 0.1$. In contrast, an island divertor uses a small but resonant radial magnetic field, $B_r/B \sim 10^{-3}$, to produce the chain of magnetic islands used for the divertor. In LHD, the connection length varies widely from field line to field line, but is also very long for most of the stochastic edge. This circumstance makes the perpendicular transport much more important than in the tokamak scrape-off layer. Whereas in tokamaks most of the heat flux across the scrape-off layer is carried to the targets by parallel heat conduction, especially in the electron channel, the perpendicular transport can in stellarators either be more or less important than the parallel one.

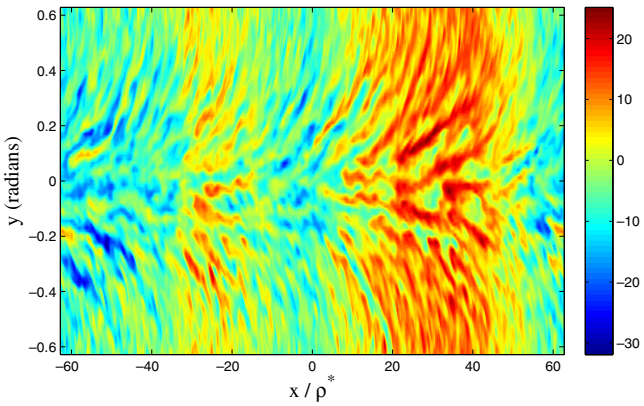

Figure 8. Snapshot of potential fluctuations in GENE simulations with adiabatic electrons of W7-X, as a function of the local radial coordinate $x = r - r_0$ and Clebsch-angle $y = \alpha = \theta - \iota\varphi$.

The greater importance of cross-field transport could be beneficial for impurity retention in the divertor [74]. Coulomb collisions between heavy impurity ions (Z) and bulk plasma ions (i) lead to two forces on the former: a friction force proportional to the velocity difference $V_{i\|} - V_{Z\|}$, which tends to flush the impurities towards the target, and a thermal force proportional to the bulk-ion temperature gradient $\nabla_\| T_i$, which drives the impurities towards the hot core plasma. In tokamaks, the latter force tends to be stronger, but in stellarators numerical modelling suggests that a friction-dominated regime is accessible in LHD as well as in W7-AS and W7-X [75].

Another obvious difference between the poloidal divertor in a tokamak and the island divertor in a stellarator is that the latter have many more X-points, which, in contrast to the tokamak, are not axisymmetric but are wound around the torus. Regions of strong plasma radiation tend to be located in the vicinity of such points, perhaps because the wider flux-surface separation reduces the cross-field heat flux, and the larger number of X-points thus help to spread the radiation more evenly over the first wall. On the other hand, the very fact that stellarators are non-axisymmetric of course makes the radiation pattern, as well as the divertor heat flux, toroidally non-uniform.

Numerical simulations [76] suggest that about 3/4 of the power in W7-AS could be radiated away by carbon impurities outside the separatrix, and even higher radiative fractions were recorded experimentally [11]. This is in stark contrast to tokamaks, where such strong radiative losses are associated with MARFE formation resulting in highly localized deposition, and where much of the radiation originates from inside the separatrix.

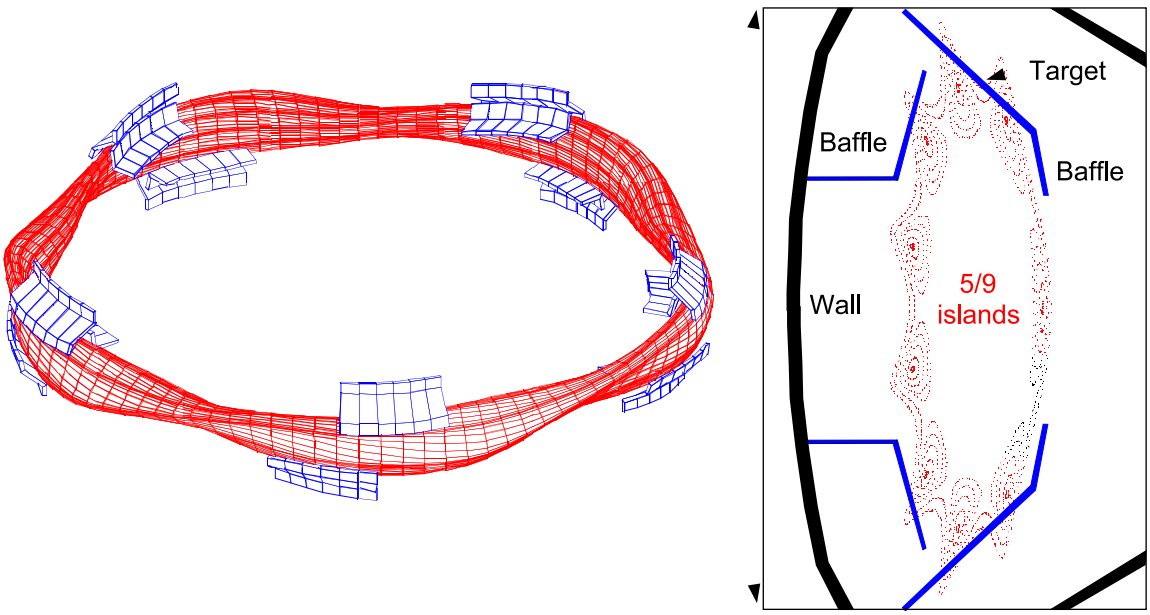

Figure 9. The island divertor of W7-AS.

The edge magnetic structure in helical devices is determined by the rotational transform in the edge region. Because of the low shear in W7-X, a resonant field of order $\delta B/B \sim 10^{-4}$–10^{-3} can generate divertor-relevant islands. Any additional perturbation field of the same order, either from error fields or from plasma currents, can modify the island structure significantly. In addition, the radial location of the resonance on which the divertor island resides is sensitive to the net toroidal plasma current, and thus to the bootstrap current. Thus, error-field compensation and plasma current control are essential for the island divertor, whereas a divertor with larger shear and a stronger, richer intrinsic field spectrum like the LHD divertor should be more robust against variations in the plasma current.

A final difference between tokamak and stellarator divertors is that the geometry of the plasma flow is more complex in the latter, making it more likely that counter-streaming plasma flows come close to each other, whereas in the tokamak the flows to the inner and outer targets are well separated. Because of the momentum exchange between such counter-streaming flows, the (thermal + kinetic) pressure need not be constant along the field. This is believed to explain why no high-recycling regime is observed in LHD or W7-AS. In W7-X, however, the islands are larger and the plasma flows around them sufficiently well separated that a high-recycling regime is predicted [74]. In contrast, one does not expect that an increase in size would sufficiently separate counter-streaming flows in a helical divertor of the LHD type. Because of the large magnetic shear, multiple island chains exist and overlap to form a stochastic zone. Overlapping islands with different mode numbers have different poloidal phases, and counter-streaming flows on neighbouring island chains approach each other *radially* at poloidal positions where they are oppositely phased.

7. Conclusions

The stellarator has both advantages and disadvantages compared with the tokamak. Intrinsic steady state and freedom from disruptions are great advantages, technical complexity a disadvantage. Macroscopic stability is better than in the tokamak, neoclassical confinement is worse, whereas turbulence and edge plasma performance are probably comparable and perhaps better. But above all, stellarator plasma physics is less well understood, and the number of possible configurations is much larger than for tokamaks. Boozer has estimated the number of degrees of freedom to be about 4 for axisymmetric systems and ∼50 for non-axisymmetric ones [77]. So far, this freedom has mainly been used to improve MHD stability and neoclassical confinement. If the remaining freedom can be exploited to reduce turbulence and optimize edge behaviour, stellarators would become even more attractive for fusion power production.

Acknowledgments

Helpful discussions with J Geiger, H Maaßberg, A Mishchenko, C Nührenberg, J Nührenberg, G Plunk and F Wagner are gratefully acknowledged. D Told and T Görler are thanked for contributing decisively to the development of the full-surface version of the GENE code. Some computations for this paper have been performed on the HPCFF cluster at the Jülich Supercomputing Center (JSC) and the Helios supercomputer in Japan.

References

[1] Spitzer L Jr 1951 *Project Matterhorn Report* PM-S-1 NYO-993, Princeton University
[2] Shafranov V D 1980 *Nucl. Fusion* **20** 1075
[3] Spitzer L 1958 *Phys. Fluids* **1** 253
[4] Mercier C 1964 *Nucl. Fusion* **4** 213
[5] Lortz D and Nührenberg J 1976 *Z. Naturf.* **31** 1277
[6] WVII-A Team 1980 *Nucl. Fusion* **20** 1093
[7] Hegna C C and Callen J D 1994 *Phys. Plasmas* **1** 3135
[8] Hayashi T, Sato T, Merkel P, Nührenberg J and Schwenn U 1994 *Phys. Plasmas* **1** 3262
[9] Narushima Y, Watanabe K Y, Sakakibara S, Narihara K, Yamada I, Suzuki Y, Ohdachi S, Oyabu N, Yamada H, Nakamura Y and LHD Experimental Group 2008 *Nucl. Fusion* **48** 075010
[10] Hegna C C 2012 *Phys. Plasmas* **19** 056101
[11] Hirsch M *et al* 2008 *Plasma Phys. Control. Fusion* **50** 053001
[12] Yamada H 2012 private communication
[13] Greenwald M 2002 *Plasma Phys. Control. Fusion* **44** R27
[14] Gates D A and Delgado-Aparicio L 2012 *Phys. Rev. Lett.* **108** 165004
[15] Cooper W A, Brocher L, Graves J P, Narushima Y and Watanabe K Y 2010 *Contrib. Plasma Phys.* **50** 713
[16] Drevlak M, Monticello D and Reimann A 2005 *Nucl. Fusion* **45** 731
[17] Kolesnichenko Ya I, Könies A, Lutsenko V V and Yakovenko Yu V 2011 *Plasma Phys. Control. Fusion* **53** 024007
[18] Grad H 1967 *Phys. Fluids* **10** 137
[19] Hudson S R and Nakajima N 2010 *Phys. Plasmas* **17** 052511
[20] Hirshman S P, van Rij W I and Merkel P 1986 *Comput. Phys. Commun.* **43** 143
[21] Hudson S R, Dewar R L, Hole M J and MacGann M 2012 *Plasma Phys. Control. Fusion* **54** 014005
[22] Dewar R L and Glasser A H 1983 *Phys. Fluids* **26** 3038
[23] McMillan B F and Dewar R L 2006 *Nucl. Fusion* **46** 477
[24] Gibson A and Taylor J B 1967 *Phys. Fluids* **10** 2653
[25] Galeev A A and Sagdeev R Z 1979 *Reviews of Plasma Physics* ed M A Leontovich (New York: Consultants Bureau) vol 7 p 307
[26] Kovrizhnykh L M 1984 *Nucl. Fusion* **24** 435
[27] Ho D D-M and Kulsrud R M 1987 *Phys. Fluids* **30** 442
[28] Mynick H E 2006 *Phys. Plasmas* **13** 058102
[29] Beidler C D *et al* 2011 *Nucl. Fusion* **51** 076001
[30] Tribaldos V and Guasp J 2005 *Plasma Phys. Control. Fusion* **47** 545
[31] Helander P 2007 *Phys. Plasmas* **14** 104501
[32] Simakov A N and Helander P 2011 *Plasma Phys. Control. Fusion* **53** 024005
[33] Sugama H, Watanabe T-H, Nunami M and Nishimura S 2011 *Phys. Plasmas* **18** 082505
[34] Sugama H, Okamoto M, Horton W and Wakatani M 1996 *Phys. Plasmas* **3** 2379
[35] Helander P and Simakov A N 2008 *Phys. Rev. Lett.* **101** 145003
[36] Sugama H and Watanabe T-H 2006 *Phys. Plasmas* **13** 012501
Sugama H and Watanabe T-H 2007 *Phys. Plasmas* **14** 079902
[37] Helander P, Mishchenko A, Kleiber R and Xanthopoulos P 2011 *Plasma Phys. Control. Fusion* **53** 054006
[38] Nührenberg J, Lotz W and Gori S 1996 *Theory of Fusion Plasmas* (Bologna: Editrice Compositori) p 3

[39] Nührenberg J and Zille R 1988 *Phys. Lett.* A **129** 113
[40] Boozer A H 1995 *Plasma Phys. Control. Fusion* **37** A103
[41] Boozer A H 1983 *Phys. Fluids* **26** 496
[42] Garren D A and Boozer A H 1991 *Phys. Fluids* B **3** 2822
[43] Landreman M and Catto P J 2011 *Plasma Phys. Control. Fusion* **53** 015004
[44] Hall L S and McNamara B 1975 *Phys. Fluids* **18** 552
[45] Gori S, Lotz W and Nührenberg J J 1996 *Theory of Fusion Plasmas* (Bologna: Editrice Compositori) p 335
[46] Nührenberg J 2010 *Plasma Phys. Control. Fusion* **52** 124003
[47] Subbotin A A *et al* 2006 *Nucl. Fusion* **46** 921
[48] Cary J R and Shasharina S 1997 *Phys. Plasmas* **4** 3323
[49] Landreman M and Catto P J 2012 *Phys. Plasmas* **19** 056103
[50] Helander P and Nührenberg J 2009 *Plasma Phys. Control. Fusion* **51** 055004
[51] Helander P, Geiger J and Maaßberg H 2011 *Phys. Plasmas* **18** 092505
[52] Turkin Y, Beidler C D, Maaßberg H, Murakami S, Tribaldos V and Wakasa A 2011 *Phys. Plasmas* **18** 022505
[53] Helander P and Sigmar D J 2002 *Collisional Transport in Magnetized Plasmas* (Cambridge: Cambridge University Press)
[54] Maaßberg H, Beidler C D and Simmet E E 1999 *Plasma Phys. Control. Fusion* **41** 1135
[55] Nührenberg J, Zille R, Mikhailov M I and Shafranov V D 2008 *Plasma Phys. Rep.* **34** 525
[56] Mynick H E, Pomphrey N and Xanthopoulos P 2010 *Phys. Rev. Lett.* **105** 095004
[57] Connor J W, Hastie R J and Taylor J B 1980 *Plasma Phys.* **22** 757
[58] Biglari H, Diamond P H and Rosenbluth M N 1989 *Phys. Fluids* B **1** 109
[59] Adam J C, Tang W M and Rutherford P H 1976 *Phys. Fluids* **19** 561
[60] Connor J W, Hastie R J and Helander P 2006 *Plasma Phys. Control. Fusion* **48** 885
[61] Proll J H E, Helander P, Connor J W and Plunk G G 2012 *Phys. Rev. Lett.* **108** 245002
[62] Kornilov V, Kleiber R, Hatzky R, Villard L and Jost G 2004 *Phys. Plasmas* **11** 3196
[63] Rewoldt G, Ku L-P and Tang W M 2005 *Phys. Plasmas* **12** 102512
[64] Xanthopoulos P and Jenko F 2007 *Phys. Plasmas* **14** 042501
[65] Watanabe T H, Sugama H and Ferrando-Margalet S 2007 *Nucl. Fusion* **47** 1383
[66] Baumgaertel J A, Belli E A, Dorland W, Guttenfelder W, Hammett G W, Mikkelsen D R, Rewoldt G, Tang W M and Xanthopoulos P 2011 *Phys. Plasmas* **18** 122301
[67] Watanabe T H, Sugama H and Nunami M 2011 *Nucl. Fusion* **51** 123003
[68] Waltz R E and Boozer A H 1993 *Phys. Fluids* B **5** 2201
[69] Kendl A, Scott B D and Wobig H 2000 *Plasma Phys. Control. Fusion* **42** L23
[70] Rafiq T, Kleiber R, Nadeem M and Persson M 2002 *Phys. Plasmas* **9** 4929
[71] Kleiber R and Scott B 2005 *Phys. Plasmas* **12** 102507
[72] Antonsen T M, Drake J F, Guzdar P N, Hassam A B, Lau Y T, Liu C S and Novakovskii S V 1996 *Phys. Plasmas* **3** 2221
[73] Peterson J L *et al* 2012 *Phys. Plasmas* **19** 056120
[74] Feng Y, Kobayashi M, Lunt T and Reiter D 2011 *Plasma Phys. Control. Fusion* **53** 024009
[75] Kobayashi M *et al* 2009 *J. Nucl. Mater.* **390–391** 325
Feng Y *et al* 2009 *Nucl. Fusion* **49** 095002
Kobayashi M *et al* 2010 *Fusion Sci. Technol.* **58** 220
[76] Feng Y, Sardei F, McCormick K, Kisslinger J and Reiter D 2006 *Nucl. Fusion* **46** 807
[77] Boozer A H 2004 *Rev. Mod. Phys.* **76** 1071